DOI: 10.1002/ejic.200901048

Ag/Graphene Heterostructures: Synthesis, Characterization and Optical Properties

Jing Li[a,b] and Chun-yan Liu*[a]

Keywords: Nanostructures / Raman spectroscopy / Surface chemistry / Reduction / Silver / Graphene

The Ag/graphene heterostructures were synthesized through a simple thermal reduction process. The interaction between Ag nanoparticles and graphene supports along with the surface plasmon resonance properties of Ag nanoparticles on graphene were investigated for the first time.

Introduction

Noble metallic (Au and Ag) nanostructures are attracting increasing interest as an important class of photonic components to control and manipulate light on the nanometer scale.[1–4] When the surface of noble metallic nanostructures is excited by electromagnetic radiation, the conductive electronic oscillations result in surface plasmon resonance (SPR) and produce surface plasmons (SPs) spread along the surface of the particles. Plasmonic excitations provide a means to focus light to subwavelength dimensions, which would overcome optical diffraction limits and enable the design of nanoscale optical devices, such as waveguides.[3,5] The intense local electromagnetic fields of metallic nanostructures accompanying plasmon resonance can also be exploited for surface enhanced spectroscopy.[6,7] The theoretical studies and experimental work have suggested that the exact position and intensity of SPR is extremely sensitive to particle size and shape, as well as to the optical and electronic properties of the medium surrounding the particles.[8–11]

Graphene (G), a monolayer of carbon atoms packed into a dense, honeycomb crystal structure, has shown fascinating properties and holds the promise for future carbon-based device architectures, owing to characteristics such as a very high carrier mobility,[12] long ballistic mean free path at room temperature,[13] and the possibility of opening a variable band gap by confinement in nanoscale ribbons.[14]

Deposition of inorganic nanoparticles, such as metals[15–18] or semiconductors,[19,20] onto G sheets would present special features in new hybrids and be useful in optical and electronic devices, catalysis, sensors, and so on. Yet, to the best of our knowledge, little attention has so far been paid to the interaction between nanoparticles and G sheets and the correlative impact on their properties. In this context, we investigated the interaction between Ag nanoparticles and G sheets by XPS (X-ray photoelectron spectroscopy) and analyzed the influence of G sheets on the surface plasmon resonance properties of Ag nanoparticles.

The route used to anchor Ag nanoparticles onto G sheets is schematically described in Scheme 1.

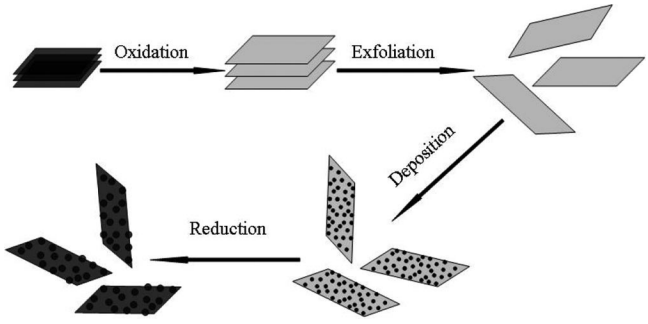

Scheme 1. The formation route to anchor Ag nanoparticles onto G sheets.

The route consists of four steps: (1) The oxidation of graphite to graphite oxide with an increased interlayer distance; (2) exfoliation of graphite oxide in water by sonication, which results in the formation of the graphene oxide (GO) dispersion; (3) deposition of Ag nanoparticles onto the graphene oxide by partial room-temperature reduction of silver ions and GO in the dispersion solution; and (4) formation of Ag/G heterostructures by further reduction of the partially reduced graphene oxide (PRGO) sheets.

Results and Discussion

A typical TEM image of Ag/PRGO heterostructures clearly shows that the almost-transparent PRGO sheets are perfectly decorated by large amounts of well-dispersed Ag

[a] Key Laboratory of Photochemical Conversion and Optoelectronic Materials, Technical Institute of Physics and Chemistry, Chinese Academy of Sciences,
Beijing 100190, PR China
Fax: +86-10-62554670
E-mail: cyliu@mail.ipc.ac.cn
[b] Graduate School of the Chinese Academy of Sciences, Beijing 100049, PR China

spherical nanoparticles (Figure 1a) and few particles reside outside of the support, which indicates the strong interaction between the Ag particles and the support. Figure 1b shows that more than 80% of the Ag particles fall in the size range 5–9 nm, and the mean particle diameter is about 8.25 nm.

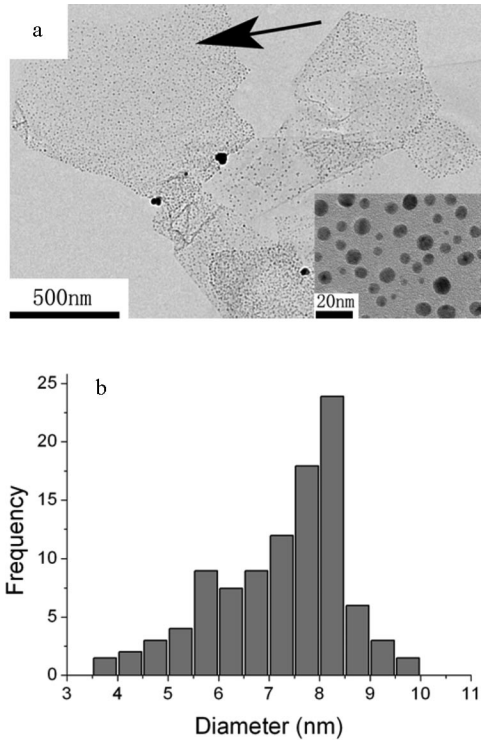

Figure 1. (a) TEM image of the Ag/PRGO heterostructures and the inset: enlarged TEM view of the area marked by an arrow; (b) the size distribution of supported Ag nanoparticles.

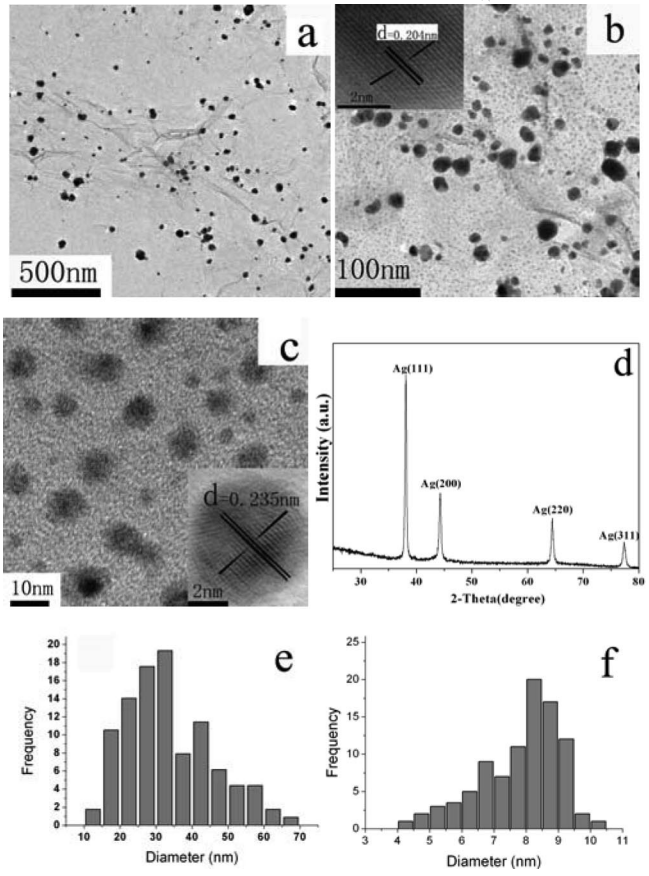

Figure 2. (a,b) TEM images of Ag/G heterostructures under different magnifications; (c) enlarged TEM image of the small particles in the background (b); (d) XRD pattern of the Ag/G heterostructures; (e) the size distribution of the bigger particles in (a); (f) the size distribution of the small particles in the background of (b). The insets in (b) and (c) show HRTEM images of the big particles and those of the small particles, respectively.

After the thermal reduction process, the resultant G sheets become more corrugated (Figure 2a), as observed previously.[15] In addition to the small particles in the G background, there is a scattering of much larger particles on the crumpled regions of the G sheets (Figure 2a and b). The average size of the large particles is about 35 nm (Figure 2e). Figure 2f depicts the size distribution of the small particles distributed in the background of Figure 2b, and the mean size is found to be 8.95 nm, which is almost the same as that in Ag/PRGO heterostructures (Figure 1b). The space fringes of the large and small particles detected in the HRTEM images (inset in Figure 2b and c) are well matched with the {200} planes and the {111} planes of Ag, respectively. The crystalline XRD pattern of the Ag/G sample (Figure 2d) matches well with that of the Ag nanoparticles (cubic, JCPDS 04-0783). The crystallite size of the Ag nanoparticles supported on G calculated from XRD is 25.5 nm, which is the mean result of both the small and large Ag particles. The large particles may be from the aggregative growth[21] of the small particles during the thermal reduction process.

In the Raman spectrum of GO [curve (a) in Figure 3], there are two prominent peaks, the D band (1355 cm^{-1}) and the G band (1600 cm^{-1}), which are usually assigned to the breathing mode of κ-point phonons of A_{1g} symmetry and the E_{2g} phonon of sp^2 C atoms, respectively.[22] After chemical reduction of GO, the ratio of the intensities of the D and G bands (I_D/I_G) increases from 0.85 to 1.10 (Table 1), which is attributed to the decrease in the mean crystallite size of G relative to that of GO. It is known that the I_D/I_G ratio is inversely proportional to the reciprocal of the average crystallite size in graphite materials.[23] The oxygen functional groups in the GO sheets can be removed by a chemical reduction, and the conjugated G network (sp^2 carbon) will be re-established. However, the size of the re-established G network is smaller than the original one, which would consequently lead to an increase in the I_D/I_G ratio.[24] In addition, the peak intensity of Ag/PRGO is higher than that of GO with a similar I_D/I_G ratio, which is due to surface-enhanced Raman scattering (SERS) from the intense local electromagnetic fields of Ag nanoparticles that accompanies plasmon resonance.

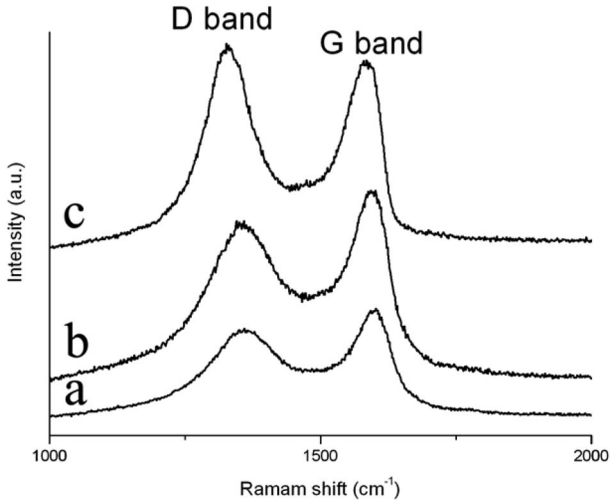

Figure 3. Raman spectra of (a) GO, (b) Ag/PRGO, and (c) Ag/G.

Table 1. The position of G band and values of I_D/I_G obtained by Raman spectroscopy.

Samples	G band position (cm^{-1})	I_D/I_G
GO	1600	0.85
Ag/PRGO	1596	0.89
Ag/G	1585	1.10

The C1s XPS spectrum of GO (Figure 4a) clearly indicates a considerable oxidation degree with different oxygenated functional groups: 286.3 eV for the expoxy and hydroxyl carbon atoms, which are located at the basal planes of the G sheets, and 287.5 eV for the carbonyl carbon atoms, which are located at the edges of the G sheets.[25] In contrast with GO, the intensity of the oxygenated functional groups in Ag/PRGO became weaker (Figure 4b), which indicates the partial reduction of GO. After thermal reduction, the intensity of the oxygenated functional groups in the C1s spectra (XPS) of Ag/G shows a significant decrease (Figure 4c), which confirms that most of the epoxy, hydroxy, and carboxyl functional groups are successfully removed. This observation is in agreement with that found in previous studies.[15,25,26]

The electronic properties of the Ag nanoparticles supported on G sheets was investigated by Ag $3d_{5/2}$ XPS. The binding energy of Ag $3d_{5/2}$ for pure Ag is 368.1 eV (Figure 5a), consistent with the standard binding energy of Ag $3d_{5/2}$ for bulk Ag.[27] The binding energy of Ag $3d_{5/2}$ for the Ag/G heterostructures is 367.5 eV (Figure 5b), which shifts remarkably to lower energy as a result of electron transfer from metallic Ag to the G sheets. Because the work function of Ag (4.2 eV)[28] is smaller than that of G (4.48 eV),[29] electron transfer from the Ag to G sheets would occur during the formation of the Ag/G heterostructures. Additionally, the interaction between the Ag and the carboxyl (C=O) groups on the edge of the G sheets also contributes to the electron transfer.[30] The binding energy of the higher ionic state of Ag is lower than that of zero-valent Ag,[27] which is peculiar for Ag. This peculiarity is attributed to shifts

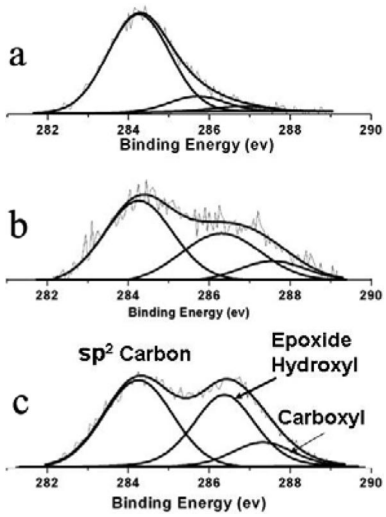

Figure 4. C1s XPS spectra of (a) GO, (b) Ag/PRGO, and (c) Ag/G.

in the initial-state potential of ionic charge and the lattice potential.[31] Therefore, in our XPS experiments, the binding energy of Ag $3d_{5/2}$ shifts to a lower value.

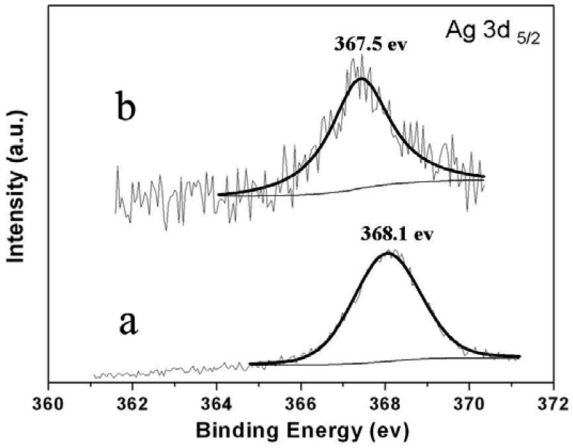

Figure 5. Ag $3d_{5/2}$ XPS spectra of (a) pure Ag and (b) Ag/G heterostructures.

The UV/Vis spectrum of GO exhibits two characteristic peaks, a maximum at 230 nm, which corresponds to π→π* transitions of aromatic C–C bonds, and a shoulder at 303 nm, which is attributed to n→π* transitions of C=O bonds (Figure 6a).[32] The peak at 230 nm is redshifted to 262 nm after the thermal reduction treatment (Figure 6b), which is an indication of the restoration of the electronic conjugation within the G sheets.[33]

According to our previous work,[34–36] the surface plasmon band of pure Ag nanoparticles (ca. 10 nm) synthesized by the reduction with borohydride is at 390 nm. Comparatively, the surface plasmon band of Ag nanoparticles in the Ag/G heterostructures is redshifted to 422 nm (Figure 6b), which is mainly due to the change in the dielectric environment and the electron density of the Ag nanoparticles in-

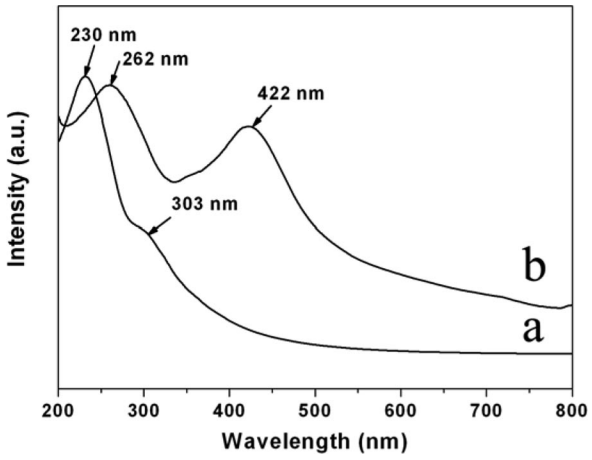

Figure 6. UV/Vis absorption spectra of (a) GO and (b) Ag/G heterostructures.

duced by the G sheets. According to the Drude model,[37] the surface plasmon band position λ is related to the effective dielectric constant of the surrounding medium:

$$\lambda^2 = \lambda_p^2(\varepsilon^\infty + 2\varepsilon_{eff})$$

where λ is the position of the plasmon band, ε^∞ is the high frequency dielectric constant as a result of interband and core transitions, ε_{eff} is the effective dielectric constant of the surrounding media, and λ_p is the metallic bulk plasma wavelength, which can be written as:

$$\lambda_p^2 = 4\pi^2c^2m\varepsilon_0/Ne^2$$

where N is the electron density of the metal core, m is the effective mass of the electron, ε_0 is the vacuum dielectric constant, and c is the velocity of light in vacuo. Because the refractive index of G ($n_{graphene}$ = 1.6–2.0) is higher than that of water (n_{water} = 1.33), the G support would induce an increase in ε_{eff} (= n^2) and result in the redshift of the surface plasmon band. Additionally, charge transfer from the Ag nanoparticles to the G support would lead to a decrease in N, which induces the redshift of the surface plasmon band. Moreover, the size increase also contributes to the redshift of the surface plasmon band.[38]

Conclusions

We have synthesized Ag/G heterostructures through the thermal reduction of Ag/PRGO, which was prepared by the room-temperature solution reduction of silver ions and the GO dispersion solution. The decrease in electron density of the Ag core and the increase in the effective dielectric constant of the surrounding media induced by the G sheets result in the redshift of the Ag surface plasmon band.

Experimental Section

Preparation of GO Dispersion Solution: Graphite oxide prepared from natural graphite powders (Beijing Chemical Factory of China) by Hummer's method[39] was used as the starting material to prepare a GO dispersion. In a typical procedure, graphite oxide (50 mg) was dispersed in water (50 g). After sonication for 1 h using a JK-300 ultrasonic cleaner (300 W, 40 kHz), we obtained a clear, brown dispersion of GO, which consisted of a hexagonal ring-based carbon network with both sp^2-hybridized carbon atoms and sp^3-hybridized carbon atoms bearing hydroxy- and epoxy functional groups on either side of the sheet. The sheet edges are mostly decorated by carboxyl groups (Figure 7). Deoxygenation of GO was accomplished by subsequent chemical reduction, whereupon a significant fraction of the bound oxygen is removed and the conjugated G network is re-established.

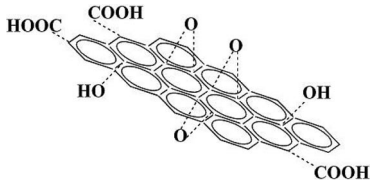

Figure 7. The chemical structure of GO.

Preparation of Ag/PRGO Heterostructures: Ag/PRGO heterostructures were prepared by the reduction of silver ions in the GO dispersion solution. Typically, an $AgNO_3$ solution (2 mL, 0.01 M) was added to the GO solution (20 mL, 0.25 mg/mL) whilst magnetically stirring for 30 min. Subsequently, an alkaline solution of sodium borohydride (pH = 9.5, 10 mL, 0.8 mg/mL) was added to the GO solution whilst stirring vigorously at room temperature for 2 h. A clear brown dispersion of Ag/PRGO was formed.

Preparation of Ag/G Heterostructures: An alkaline solution of sodium borohydride (pH = 9.5, 20 mL, 25 mg/mL) was added to the brown Ag/PRGO dispersion solution whilst stirring vigorously. The solution was kept at 80 °C for 1 h under a nitrogen atmosphere. The color of the dispersion solution changed from brown to black, which was previously suggested as resulting from the partial restoration of the network within the carbon structure as a result of the reduction of GO.[25]

Characterization: The TEM images were taken with a JEM 2100F transmission electron microscope, by using an accelerating voltage of 200 kV. The samples were dispersed in deionized water by sonication and dropped onto a conventional carbon-coated copper grid. The XRD pattern was obtained with a Bruker D8 Focus under Cu-K_α radiation at 1.54056 Å with a scanning speed of 4°/min. The Raman spectrum was recorded with a Via-Reflex Raman system, by using a 532-nm excitation wavelength. The XPS measurements were performed on a MICROLAB MK II spectrophotometer with Mg-K_α radiation. UV/Vis absorption spectra were recorded with a Shimadzu UV-1601 PC spectrophotometer. The samples were dispersed in deionized water for optical measurements.

Acknowledgments

The authors are grateful for the support from the Chinese Academy of Sciences and for the 973 Program.

[1] T. W. Ebbesen, H. J. Lezec, H. F. Ghaemi, T. Thio, P. A. Wolff, *Nature* **1998**, *391*, 667–669.
[2] J. B. Pendry, *Phys. Rev. Lett.* **2000**, *85*, 3966–3969.
[3] S. A. Maier, M. L. Brongersma, P. G. Kik, S. Meltzer, A. A. G. Requicha, H. A. Atwater, *Adv. Mater.* **2001**, *13*, 1501–1505.
[4] S. A. Maier, P. G. Kik, H. A. Atwater, S. Meltzer, E. Harel, B. E. Koel, A. A. G. Requicha, *Nat. Mater.* **2003**, *2*, 229–232.

[5] W. L. Barnes, A. Dereux, T. W. Ebbesen, *Nature* **2003**, *424*, 824–830.
[6] S. Nie, S. R. Emory, *Science* **1997**, *275*, 1102–1106.
[7] K. Kneipp, Y. Wang, H. Kneipp, L. T. Perelman, I. Itzkan, R. R. Dasari, M. S. Feld, *Phys. Rev. Lett.* **1997**, *78*, 1667–1670.
[8] M. Kerker, *The Scattering of Light and Other Electromagnetic Radiation*, Academic Press, New York, **1969**.
[9] C. F. Bohren, D. R. Huffman, *Absorption and Scattering of Light by Small Particles*, Wiley, New York, **1983**.
[10] A. Henglein, *J. Phys. Chem.* **1993**, *97*, 5457–5471.
[11] P. Mulvaney, *Langmuir* **1996**, *12*, 788–800.
[12] K. S. Novoselov, A. K. Geim, S. V. Morozov, D. Jiang, Y. Zhang, S. V. Dubonos, I. V. Grigorieva, A. A. Firsov, *Science* **2004**, *306*, 666–669.
[13] C. Berger, Z. Song, X. Li, X. Wu, N. Brown, C. Naud, D. Mayou, T. Li, J. Hass, A. N. Marchenkov, E. H. Conrad, P. N. First, W. A. de Heer, *Science* **2006**, *312*, 1191–1196.
[14] Z. Chen, Y. M. Lin, M. J. Rooks, P. Avouris, *Phys. E* **2007**, *40*, 228–232.
[15] C. Xu, X. Wang, J. W. Zhu, *J. Phys. Chem. C* **2008**, *112*, 19841–19845.
[16] R. Muszynski, B. Seger, P. V. Kamat, *J. Phys. Chem. C* **2008**, *112*, 5263–5266.
[17] B. S. Kong, J. X. Geng, H. T. Jung, *Chem. Commun.* **2009**, *16*, 2174–2176.
[18] M. A. Hassan, V. Abdelsayed, A. E. R. S. Khder, K. M. Abou-Zeid, J. Terner, M. S. El-Shall, S. I. Al-Resayes, A. A. El-Azhary, *J. Mater. Chem.* **2009**, *19*, 3832–3837.
[19] G. Williams, B. Seger, P. V. Kamat, *ACS Nano* **2008**, *2*, 1487–1491.
[20] G. Williams, P. V. Kamat, *Langmuir* **2009**, *25*, 13869–13873.
[21] S. Kumar, T. M. Davis, H. Ramanan, R. L. Penn, M. Tsapatsis, *J. Phys. Chem. B* **2007**, *111*, 3398–3403.
[22] F. Tuinstra, J. L. Koenig, *J. Chem. Phys.* **1970**, *53*, 1126–1130.
[23] M. A. Pimenta, G. Dresselhaus, M. S. Dresselhaus, L. G. Cancado, A. Jorio, R. Saito, *Phys. Chem. Chem. Phys.* **2007**, *9*, 1276–1290.
[24] G. Wang, J. Yang, J. Park, X. Gou, B. Wang, H. Liu, J. Yao, *J. Phys. Chem. C* **2008**, *112*, 8192–8195.
[25] S. Stankovich, D. A. Dikin, R. D. Piner, K. A. Kohlhaas, A. Kleinhammes, Y. Y. Jia, Y. Wu, S. T. Nguyen, R. S. Ruoff, *Carbon* **2007**, *45*, 1558–1565.
[26] Y. Zhou, Q. L. Bao, L. A. L. Tang, Y. L. Zhong, K. P. Loh, *Chem. Mater.* **2009**, *21*, 2950–2956.
[27] J. F. Moudler, W. F. Stickle, P. E. Sobol, K. D. Bomben, *Handbook of X-ray Photoelectron Spectroscopy*, Perkin–Elmer, Eden Prairie, MN, **1992**.
[28] I. Lopez-Salido, D. C. Lim, R. Dietsche, N. Bertram, Y. D. Kim, *J. Phys. Chem. B* **2006**, *110*, 1128–1136.
[29] X. J. Wu, X. C. Zeng, *Nano Lett.* **2009**, *9*, 250–256.
[30] Z. W. Deng, M. Chen, L. M. Wu, *J. Phys. Chem. C* **2007**, *111*, 11692–11698.
[31] R. Vinu, G. Madras, *Appl. Catal. A: Gen.* **2009**,*366*, 130–140.
[32] J. I. Paredes, S. Villar-Rodil, A. Martı′nez-Alonso, J. M. D. Tascón, *Langmuir* **2008**, *24*, 10560–10564.
[33] D. Li, M. B. Muller, S. Gilje, R. B. Kaner, G. G. Wallace, *Nat. Nanotechnol.* **2008**, *3*, 101–105.
[34] L. Zang, C. Y. Liu, X. M. Ren, *J. Photochem. Photobiol. A: Chem.* **1993**, *74*, 267–271.
[35] L. Zang, C. Y. Liu, X. M. Ren, *J. Chem. Soc., Chem. Commun.* **1995**, *4*, 447–448.
[36] L. Zang, C. Y. Liu, X. M. Ren, *Acta Chim. Sinica* **1994**, *52*, 588–594.
[37] P. Mulvaney, *Langmuir* **1996**, *12*, 788–800.
[38] A. Henglein, *Langmuir* **2001**, *17*, 2329–2333.
[39] W. Hummers, R. Offeman, *J. Am. Chem. Soc.* **1958**, *80*, 1339.

Received: October 29, 2009
Published Online: February 2, 2010

